Phase transitions in open quantum systems: the MIPT and the BTC phenomenon

Siddhant Midha
Department of Electrical Engineering
Indian Institute of Technology Bombay
siddhant-midha.github.io/

Last Updated: January 1, 2024

Abstract

This report summarizes my study of trajectory-level open quantum system dynamics. It details the continuous time crystal phase and the measurement-induced phase transition exhibited in monitored many-body systems. This document contains notes, reviews, and some simulations I performed. Original research resulting as a part of this study will be outlined in a paper.

Contents

§0. Introduction: Open system dynamics

A basic postulate of quantum mechanics states that *closed* quantum systems are described by a wave-function Ψ, which evolves according to the (in-)famous Schrödinger equation,

$$\imath\hbar\frac{\partial}{\partial t}\Psi = \mathcal{H}\Psi \tag{0.1}$$

Albeit, isolating quantum systems is hard, and the process of it has gotten experimentalists around the world burning the night oil. Thus, us theorists have to step up and contribute. This effort recognizes that most quantum systems are *open*, with some coupling to a *bath* or an environment [1]. Such a coupling leads to an effective description of the principle system of interest with a density-matrix, rather than a wave-function. Formally, given a system S coupled to an environment E, one can assume a wave-function description of the total SE system $|\psi\rangle_{SE}$, and upon tracing out the environment we gain a density matrix description of the system,

$$\rho_S := \mathrm{tr}_E(|\psi\rangle_{SE}\langle\psi|_{SE}) \tag{0.2}$$

Much work has gone into the development of theoretical tools to describe open system dynamics, where careful approximations on the nature of the system-bath coupling lead to closed-form equations for the system density matrix [BP02; WM09].

Let us know discuss a bit more about the formalism. Assuming that the initial state of the system-environment is $\rho_S \otimes \rho_E$ (i.e., no correlations exist *initially*, the initial state is factorized), the state after unitary evolution U is

$$\rho'_{SE} = U(\rho_S \otimes \rho_E)U^\dagger \tag{0.3}$$

Assume that the initial environment state was

$$\rho_E = \sum_k p_k |\phi_k\rangle\langle\phi_k| . \tag{0.4}$$

Now, if we measure the environment operator

$$R = \sum_n r_n |\varphi_n\rangle\langle\varphi_n| \tag{0.5}$$

and get the measurement result n, then an application of the von-Neumann projective measurement principle tells us that the resulting system state (i.e., after the partial trace) is

$$\rho_S^{(n)\prime} = \frac{\sum_k \Omega_{nk}\rho_S\Omega_{nk}^\dagger}{\mathrm{Tr}(\sum_k \Omega_{nk}\rho_S\Omega_{nk}^\dagger)} \tag{0.6}$$

[1] I believe the term 'bath' is used to refer to an environment with infinite degrees of freedom, while 'environments' in general can be engineered. Being pedantic, of course

where $\Omega_{nk} = \sqrt{p_k}\langle\varphi_n|U|\phi_k\rangle$ is the set of *Kraus* operators emergent from the dynamics. The equation 0.6 describes *selective* measurement, and informs about the state if the measurement result is n. The *non-selective* outcome instead is,

$$\rho_S' = \sum_n P(n)\rho_S^{(n)\prime} = \sum_{nk} \Omega_{nk}\rho_S\Omega_{nk}^\dagger \tag{0.7}$$

If one may quote Breuer and Petruccione then, "... the first important step in the description of an open quantum system is to make clarity about the type of measurement which is performed in order to obtain information ...". It is crucial as this distinction indeed dictates which formalism must be used to describe the statistical properties of such an open quantum system. Moreover, the set

$$\{\Omega_{nk}\}_{nk} \tag{0.8}$$

forms an *operator-sum* or *Kraus* representation of the open system dynamics, and is one tool that is used to discuss such systems. Particularly, we will refer to this formalism while discussing the 'traditional' random quantum circuit setting of the MIPT. For now, we move on to the Lindblad and quantum trajectory methods.

The Lindblad master equation (LME) method proves to be a ubiquitous tool in describing continuous time open system evolution. Assuming Markovian dynamics ($\tau_B\tau_R$: bath correlation times are much smaller than system relaxation times) one finds that the system state must evolve as,

$$\rho_S(t) = V(t)\rho_S(0) \tag{0.9}$$

with $V(t) : \mathcal{D}(\mathcal{H}_S) \to \mathcal{D}(\mathcal{H}_S)$ is a family of dynamical maps satisfying the semi-group property

$$V(t_1 + t_2) = V(t_1)V(t_2) \tag{0.10}$$

This must take the form $V(t) = \exp\{\mathcal{L}t\}$, implying,

$$\frac{d\rho}{dt} = \mathcal{L}\rho \tag{0.11}$$

Then we impose

$$\mathcal{L}\rho_S := \lim_{\epsilon\to 0} \frac{V(\epsilon)\rho - \rho}{\epsilon} \tag{0.12}$$

on the operator-sum formalism, which finally gives us after some algebra,

$$\mathcal{L}\rho = -\iota[\mathcal{H},\rho] + \sum_{k=1}^{N^2-1} \gamma_k \mathcal{D}[A_k]\rho \tag{0.13}$$

where,

$$\mathcal{D}[A]\rho := A\rho A^\dagger - \frac{1}{2}\left(A^\dagger A\rho + \rho A^\dagger A\right) \tag{0.14}$$

where the $N^2 - 1$ dissipative terms result from the N^2 Kraus operators. This LME neatly separates the Hamiltonian and dissipative terms of the open system

evolution, and one can easily simulate this deterministic differential equation. For instance, for describing continuous time crystals, we would have $\mathcal{H} \propto J_x$ and $A \propto J_-$, and one can easily study the CTC phenomenon using the LME equation. One must keep in mind that this is a description of the *average* density matrix, wherein the measurement results are forgotten (non-selective measurement) — that is, the possible measurement outcomes are summed over with their respective probabilities, which can also be obtained by summing over all the Kraus operator terms $\Omega_{nk}\rho\Omega_{nk}^\dagger$. For instance, for some driven system of bosons, if the quadrature operators $x_- = a + a^\dagger$ are being measured, one can enter $A := x_-$ to study the average density evolution. But, this does not provide access to the measurement results, and thus decreases purity. That is why the LME description cannot be used to study MIPT. Now, we describe what is known as *unravellings* of the LME. Given such an average equation, there can be multiple stochastic wave-function level unravellings which lead to the same average dynamics. We discuss the jump and diffusion unravellings in particular.

§1. The Measurement Induced Phase Transition

§§1.1. Introduction: MIPT in RQCs

The nature of entanglement in quantum many-body systems has been crucial for understanding many dynamical and phase-transition phenomenon in quantum systems. One important class of such systems are monitored quantum systems, which are being continuously observed by (or dissipated into) the environment. Different behaviours have been observed in integrable and non-integrable (chaotic) quantum systems as the strength of measurement is varied. This is manifested in the scaling of entanglement in a quantum system with the size N of the system. Notably, in the *area law* phase, the entanglement of a state is $\mathcal{O}(1)$, and in the *volume law* phase, the entanglement of a state is $\mathcal{O}(N)$.

In [CTDL19], the authors observed the absence of a stable volume-law phase under the presence of any monitoring, i.e., the dynamics saturate to an area-law behaviour for any arbitrarily small amount of measurement. In stark contrast, [LCF18], outline how in the setting of brick-wall random quantum circuits perturbed by measurements, (a chaotic system) there is a finite measurement strength p_c uptill when the volume-law survives. We take this as the starting point of studying the so called *measurement induced quantum phase-transition* (MIPT), with random unitary circuits being our first playground.

The model under study is shown in Fig. 1. This is a brick-wall circuit, which consists of random unitaries U interdispersed by measurements with probability p. Open boundary conditions are considered. With a lattice consisting of an even number of qubits, the evolution is formally described for even and odd time steps as follows. For t even, define the unitary

$$\mathcal{U}_e := \Pi_i U_{2i,2i+1} \tag{1.1}$$

and for t odd, define,

$$\mathcal{U}_o := \Pi_i U_{2i-1,2i} \tag{1.2}$$

with the individual two-qubit unitaries U being drawn from a random ensemble. This could be the from Haar measure, or from the set of random Clifford gates. Now, let K_i denote the probabilistic measurement of qubit i, which with probability $1-p$ does nothing, and with probability p measures the qubit i in the computational Z basis. Thus, we define the net evolution operator at time step t as,

$$\mathcal{E}_t := (\Pi_i K_i)\mathcal{U}_\alpha,\ \alpha \in \{e, u\} \tag{1.3}$$

Note that this is equivalent to the way [LCF18] performs rank-1 measurements. We evolve the system with such dynamics, and ask the question about the entanglement dynamics of the evolved quantum trajectories $\{|\Psi(t)\rangle\}$ for times $t \in \{1, 2, \ldots, 2N\}$ where N is the size of the system. The results of the entanglement dynamics are shown in Fig. 2. For $p = 0$, we observe a linear increase in the entanglement entropy up untill a saturation value, and note that the saturated entropy is volume law – it scales linearly with N. As p is increased, this

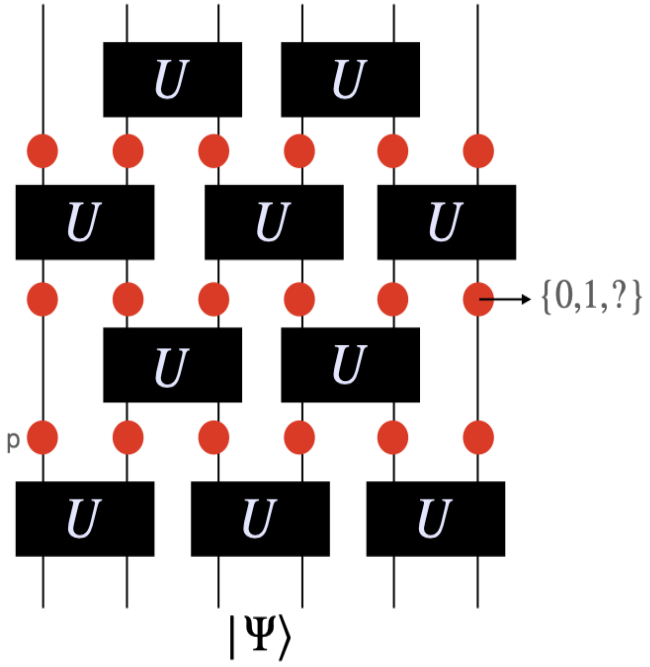

Figure 1: The typical playground for the MIPT: The *brickwall* random quantum circuit, consisting of random unitaries U sampled independently from, say, the Haar measure, and intermittent projective measurements (red dots) which occur with a probability p. The output from a single red dot is formally is in $\{0, 1, ?\}$, with it being ? with probability $1 - p$ when a measurement does not happen. Also, $p(0) + p(1) = p$.

saturation value decreases, and for $p = 0.2$, the saturation value becomes $\mathcal{O}(1)$, i.e., indepedent of N. Thus, we establish a the existence of a transition from volume-law to area-law. Also, as we vary the strength of the measurements p, we notice that the time taken for the entanglement to saturate to it's steady values reduces from $\sim 2N$ in the $p = 0$ case to $\mathcal{O}(1/p)$ in the $p > p_c$ case.

Now, how do we find the critical point p_c? We can do this in two ways. One, by noting the variation of the entropy on N for different values of p. The critical value will be when the plot of $\mathcal{E}$ v.s. N is a horizontal line. Another way is to plot the long-term entropy as a function of p for different values of N, which should lead to a collapse in the plots at $p \approx p_c$. We do this for a **single** trajectory in Fig.3, and the plots (a) and (b) indicate that $p \approx p_c$. We further aim to quantify this by employing the scaling ansatz

$$S_A(p, N) = L^{\gamma} F((p - p_c)N^{1/\nu}) \tag{1.4}$$

where $F(\cdot)$ is the scaling function. We can do this by plotting S_A/N^{γ} as a function of $(p - p_c)N^{1/\nu}$. We fix $p_c = 0.15$, and vary the critical exponents γ, ν to get a fit, and plot the results in Fig.3(c) for the fit $\nu = 1.84$ and $\gamma = 0.3$. Of course, this is a single trajectory so the scaling is not perfect. We average over fifty trajectories and plot the results in Fig.4, which confirm the critical point to be $p_c = 0.15$, agreeing with that from [LCF18]. One can now proceed to get more information about the scaling function [LCF18] by demanding that

$$S_A = \mathcal{O}(L_A) \text{ for } p < p_c \text{ and } S_A = \mathcal{O}(1) \text{ for } p > p_c \tag{1.5}$$

we get that $F(x) \sim |x|^{(1-\gamma)\nu}$ for $x \to -\infty$ and $F(x) \sim x^{-\gamma\nu}$ for $x \to \infty$, thereby implying

$$\lim_{N\to\infty} N^{-1} S_A(p, N) \sim |p - p_c|^{(1-\gamma)\nu} \textbf{ for } p < p_c \tag{1.6}$$

$$\lim_{N\to\infty} S_A(p, N) \sim |p - p_c|^{-\gamma\nu} \textbf{ for } p > p_c \tag{1.7}$$

In comparison with Ising models, the entropy per unit qubit serves as a density much like the magnetization which is the magnetic moment per unit site. The entropy density thus serves as an order parameter for the weak measurement phase, vanishing continuously at the critical point with exponent $(1 - \gamma)\nu \sim 4/3$.

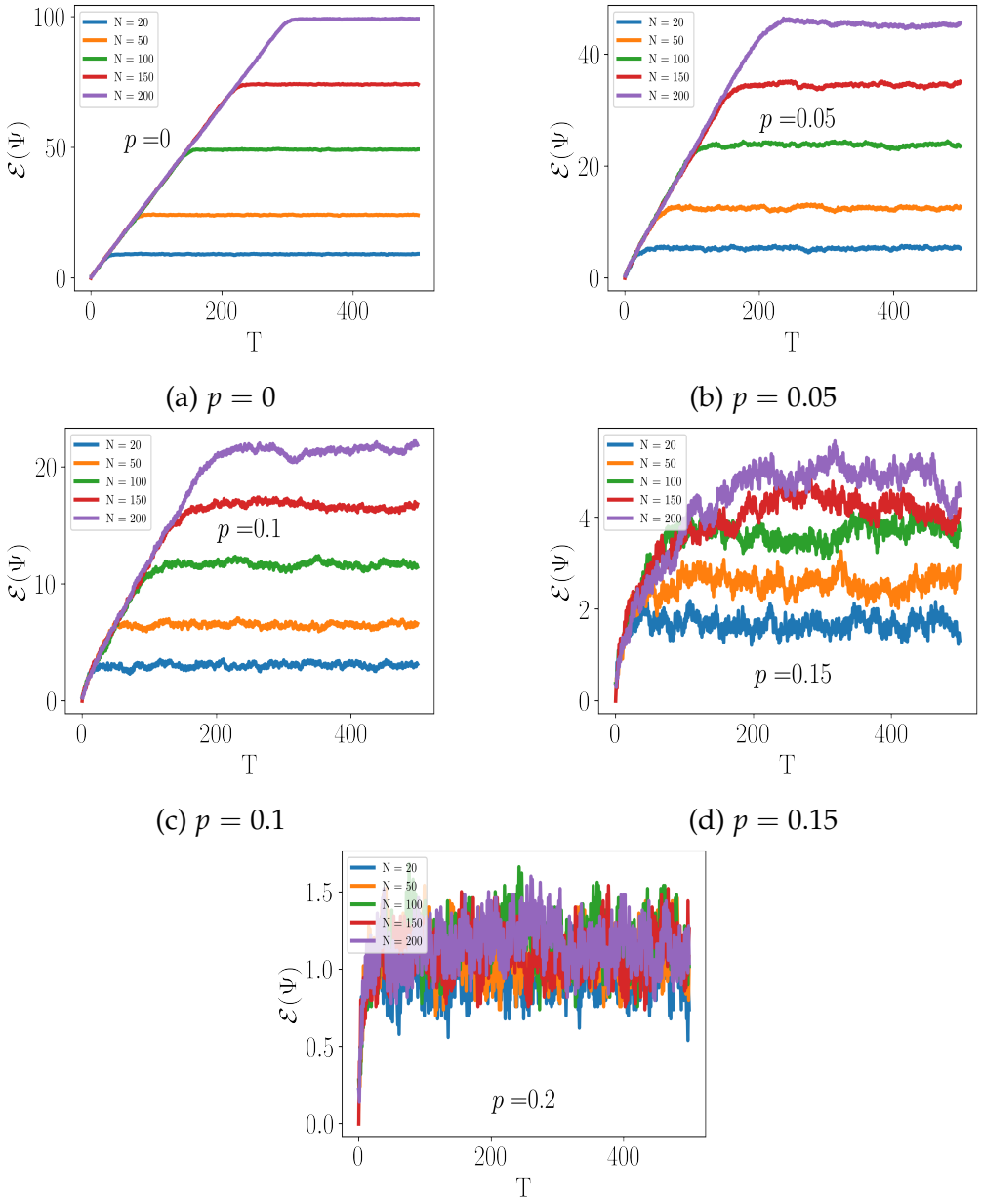

(a) $p = 0$ (b) $p = 0.05$

(c) $p = 0.1$ (d) $p = 0.15$

(e) $p = 0.2$

Figure 2: Entanglement dynamics of brickwall circuits with single-qubit projective measurements in the computational basis happening probability p. The critical measurement strength is identified as $p_c \approx 0.15$. Averaged over 50 trajectories.

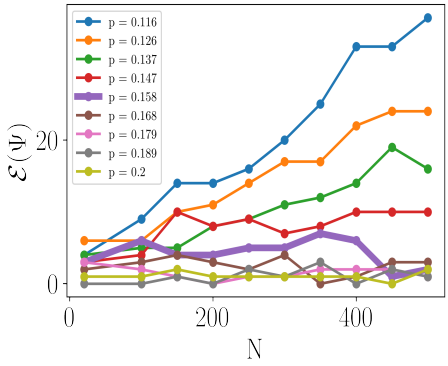

(a) As a function of N

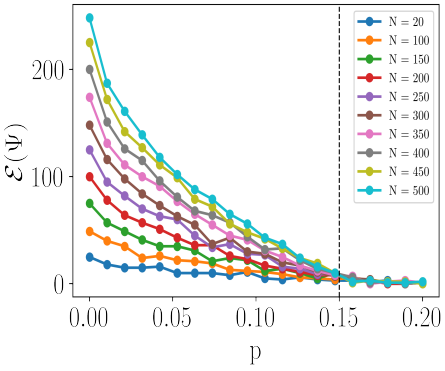

(b) As a function of p

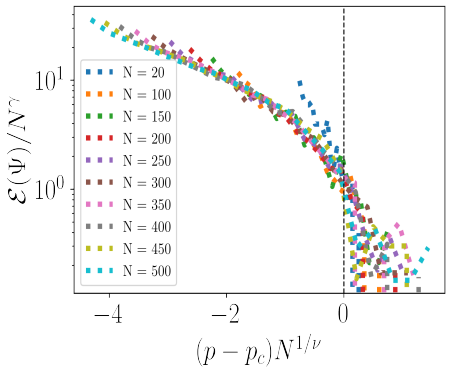

(c) Collapse

Figure 3: Long-time entanglement entropy of *single* trajectories of the brick-wall circuit. The critical value p_c can be intuitively seen to be around 0.15, but the finite N scaling is not very good.

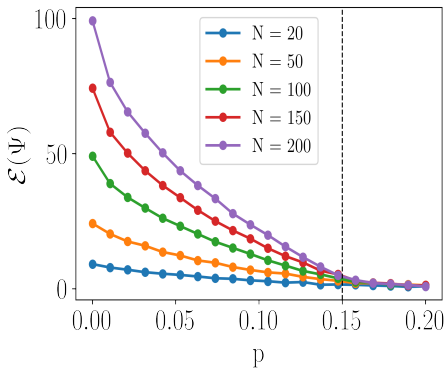

(a) As a function of N

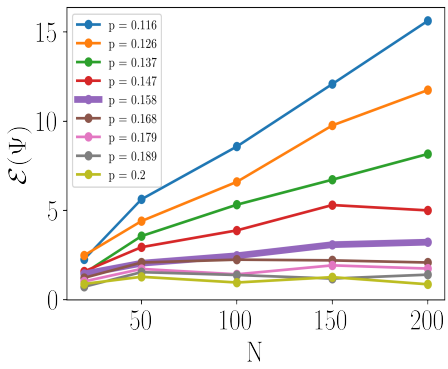

(b) As a function of p

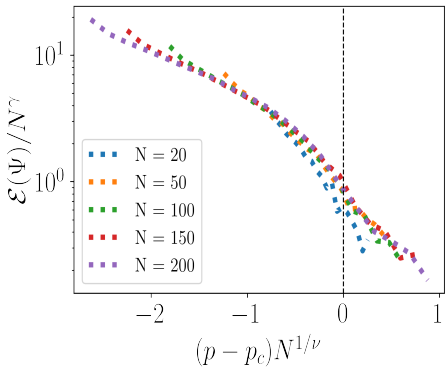

(c) Collapse

Figure 4: Long-time entanglement entropy averaged over 50 trajectories of the brick-wall circuit. The critical point $p_c = 0.15$ is identified clearly owing to the clear finite-N scaling now.

§§1.2. Interesting works

[BCA20] When one works with the MIPT, one needs to average in two levels – one over the unitaries, and one over the possible measurement outcomes. The averaged entropy (say, half-system) can then be written as,

$$S_A = \langle \sum_{i_M} p_{i_m}(U) S_A(i_M, U) \rangle_U \tag{1.8}$$

where i_M is a possible measurement outcome (a *very* long bit vector, essentially), A is a subsystem, and U is a possible circuit realization. The authors of [BCA20] take into account averaging over the i_M by writing the joint system-ancilla state (note that you can think of the ancilla as the measurement probes) as

$$\rho_{ABM} = \sum_P i_M p_{i_M} |\Psi(U, i_M)\rangle \langle \Psi(U, i_M)| \otimes |i_M\rangle \langle i_M| \tag{1.9}$$

Now, if one wants to compute the entropy $S_A(U)$ averaged over the measurements but for a particular Haar realization U, it is nothing but the conditional entropy of A on M, given as

$$S_A(U) = S(A|M) = S_{AM} - S_M \tag{1.10}$$

These are easier to compute analytically than the entropies for a particular trajectory i_M. While S_M is just the classical Shannon entropy of p_{i_M}, $S(A|M)$ is still tricky. To go around this, the authors use a replica trick to compute this by introducing $S^{(n)}(A|M) = S^{(n)}_{AM} - S^{(n)}_M$ where

$$S^{(n)}_X := \frac{\log\langle \mathrm{Tr}\, \rho^n_X \rangle_U}{1-n} \tag{1.11}$$

This quantity converges to the conditional entropy $\langle S(A|M)\rangle_U$ for $n \to 1$.

Another quantity they deal with is the Fisher information, which talks about the learnability of the quantum system in the volume-law and area-law phases. Consider $|\Psi_0\rangle$ and $|\Psi_x\rangle := \delta U(x)\,|\Psi_0\rangle$ for x small and $\delta U(x) = \exp\{-\iota A x\} \approx 1$. If one looks at the probability distributions of the outcomes p_0 and p_x one can define the average (over U) KL divergence between them as,

$$D_{KL}(p_0, p_x) := \sum_{i_M} p_{0,i_M} \log \frac{p_{0,i_M}}{p_{x,i_M}}. \tag{1.12}$$

Further, we define the Fisher information as

$$\mathcal{F} = \partial_x^2 D_{KL}(p_0, p_x)|_{x=0} \tag{1.13}$$

This quantifies the amount of information that can be learned from the system. One expects a sharp transition in this quantity from the area-law to the volume-law phases, wherein the dissipation enables the environment to learn about the system in the former, and the highly non-local distribution in the latter prevents the environment from learning about the system qubits. A similar replica trick is used. Further, the replica quantities are mapped to some exactly solvable classical statistical mechanics models to enable analytic control over MIPT (to some extent).

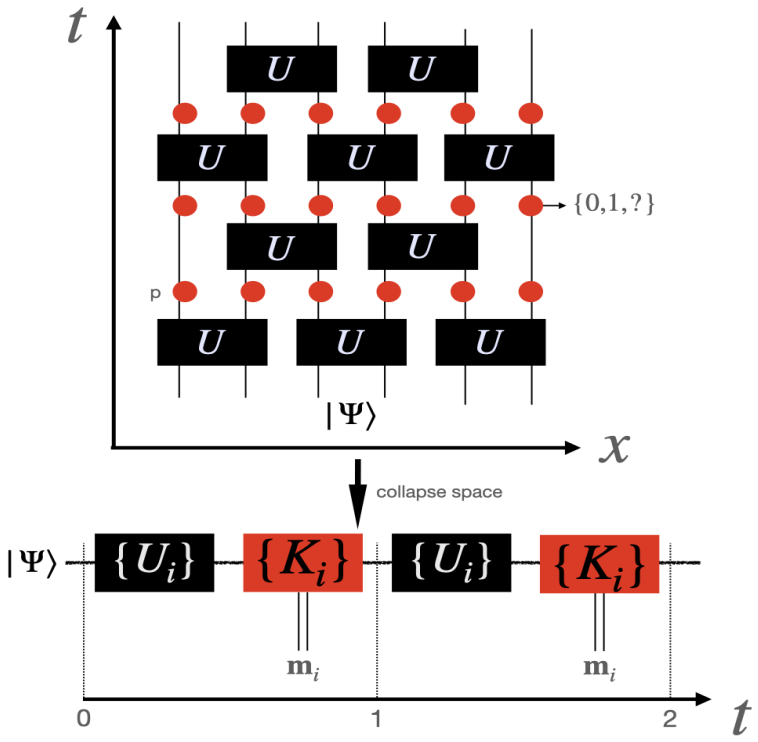

Figure 5: Alternate picture for the RQC-MIPT with a collapse of the spatial dimension. The measurement results at each time-step are $\mathbf{m}_i \in \{0, 1, ?\}^N$, where N is the number of qubits.

§2. Boundary time crystals

Time crystals are a many-body quantum phase of matter where time translational symmetry is broken [KMS19]. These phases occur in two flavours: discrete and continuous time crystals. In the former, a discrete symmetry of the drive on the system (say of frequency ω) is broken by the system showing behaviours at lower frequencies. This is symmetry breaking as a drive at ω induces oscillations at $n\omega$ for all $n \in \mathbb{N}$, but not at any $\omega_1 < \omega$. The latter, on the other hand, occurs when a system undergoing evolution under a time independent Hamiltonian shows persistent oscillations at a frequency depending on the coupling constants, thereby breaking *continuous* time translational symmetry. We focus on the latter in this work.

The term *boundary* time crystal was coined in [Iem+18], where the idea is that, a macroscopic system of size N_b can be interpreted as the boundary of a bulk of size N_B, and the evolution of the total closed system can be written with the (time dependent) Hamiltonian

$$\hat{H}_b + \hat{H}_B + \hat{B} \tag{2.1}$$

While the closed system by itself cannot break time translational symmetry, particular Hamiltonians can cause a reduced subsystem (the boundary) to undergo persistent oscillations (limit cycles) in the thermodynamic limit of $N_b, N_B \to \infty$,

but keeping $N_b/N_B \to \infty$. The state of the entire closed system evolves unitarily,

$$|\psi(t)\rangle = e^{-\iota \hat{H} t} |\psi(0)\rangle \tag{2.2}$$

The state of the boundary can be described by

$$\hat{\rho} := \mathrm{Tr}_B[|\psi\rangle \langle\psi|] \tag{2.3}$$

and the evolution can be described using a Markovian master equation,

$$\frac{d\rho}{dt} = \mathcal{L}\rho \tag{2.4}$$

One can then have some observible $\hat{O}$ such that

$$\lim_{N_b, N_B \to \infty} \mathrm{Tr}[\hat{O}\hat{\rho}] = f(t) \tag{2.5}$$

where $f(t)$ is a time periodic function, demonstrating breaking time-translational symmetry. Thus, since the reduced matrix ρ of such a system is generally non-thermal, previous no-go theorems on time crystals do not apply, establishing that such Hamiltonian systems can spontaneously break time-translation symmetry as a boundary phase.

The paper [Iem+18] further goes on to giving a playground model for numerically studying the BTC. Consider an ensemble of N spins, and define the collective operators

$$S^\alpha := \frac{1}{2} \sum_{i=1}^{N} \sigma_i^\alpha \quad \forall \alpha \in \{x, y, z\} \tag{2.6}$$

Then consider a system driven with a frequency Ω but with the time dependence gauged away, leading to the Hamiltonian $\mathcal{H} = \Omega S^x$. Further consider collective dissipation of the spins, which can be formally described by the operator S^-, and thus the dynamics can be written down as,

$$\frac{d\rho}{dt} = -\iota\Omega[\rho, S^x] + \frac{\kappa}{S}\mathcal{D}[S^-]\rho \tag{2.7}$$

where $S := N/2$ is the total spin, and κ is the rate of dissipation, which is normalized by the total spin S. It is pointed out that the specific form of the bulk Hamiltonian $\mathcal{H}_B$ does not matter, only the effective Lindblad dynamics does.

This model shows a dissipative phase transition at $\Omega/\kappa = 1$, with $\Omega/\kappa < 1$ being the dissipative phase, and $\Omega/\kappa > 1$ being the time crystal phase. The former shows a decay of the total magnetization to $-N/2$ even in the thermodynamic limit, while the latter shows limit-cycles.

We now show numerical results to support these arguments. We plot the dynamics of the expected magnetization in the z-direction in Fig.6 and 7, with the former for the dissipative phase and critical point and the latter for the time

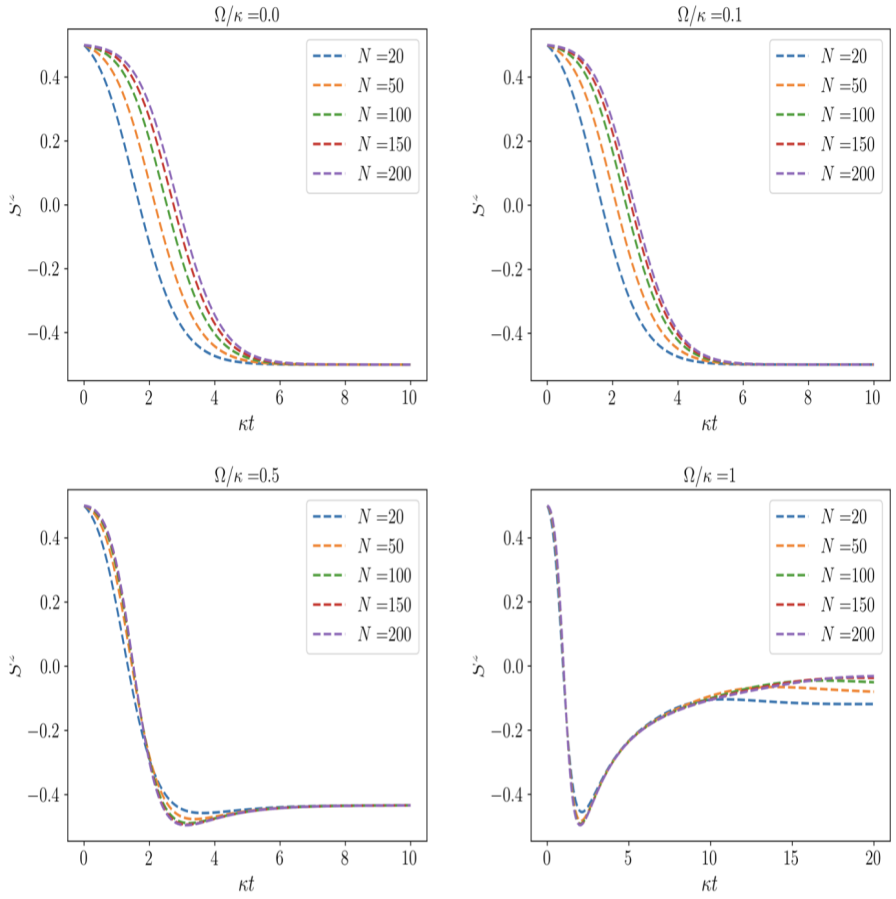

Figure 6: Time dynamics of the $z-$projected spin for $N \in \{20, 50, 100, 150, 200\}$ for $\Omega/\kappa \in \{0, 0.1, 0.5, 1.0\}$

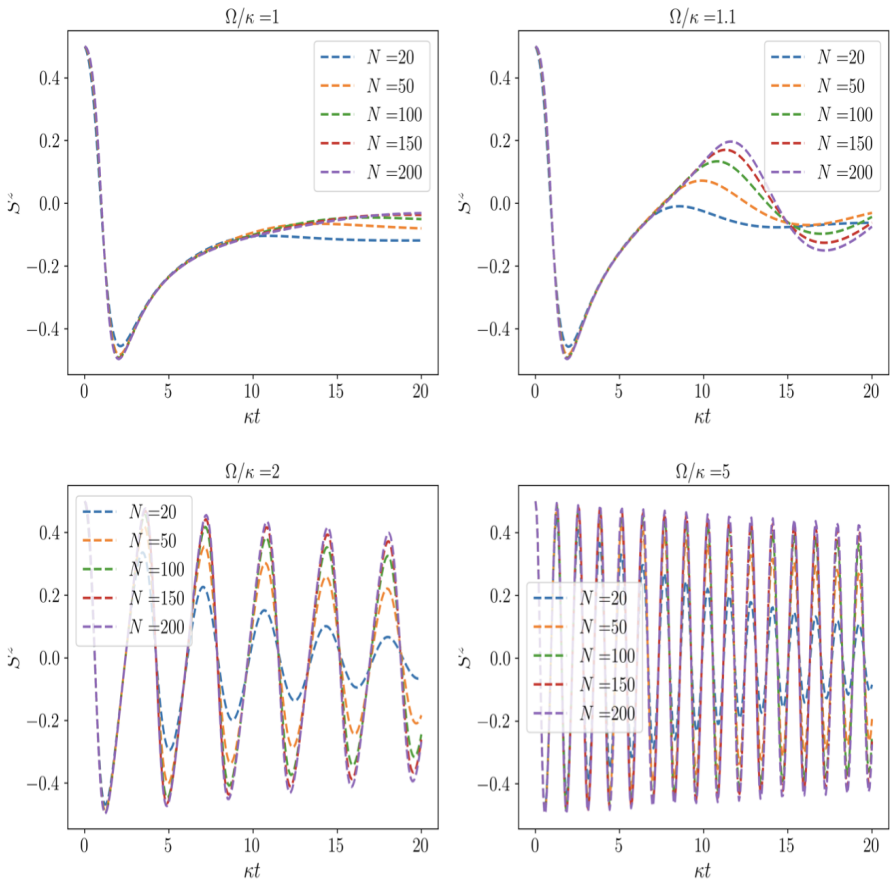

Figure 7: Time dynamics of the $z-$projected spin for $N \in \{20, 50, 100, 150, 200\}$ for $\Omega/\kappa \in \{1.1, 2, 10\}$

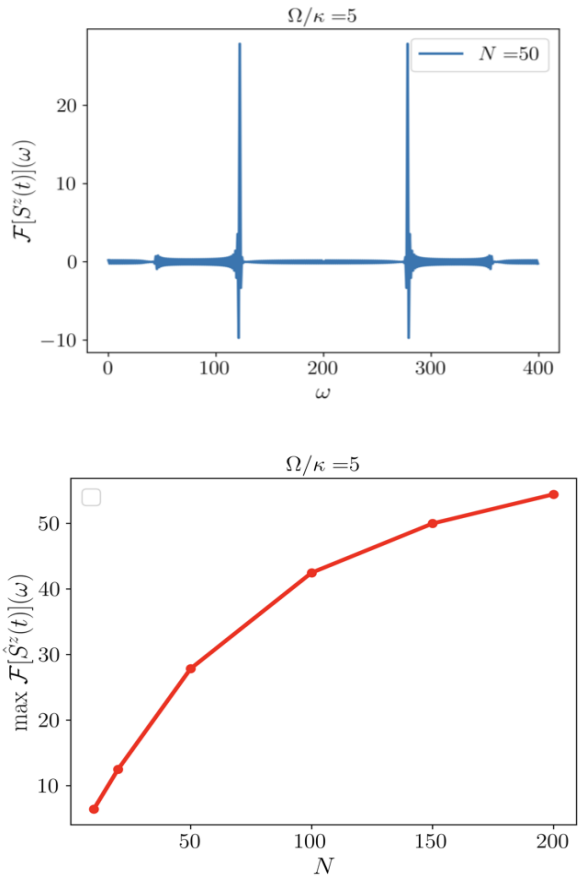

Figure 8: Fourier dynamics of the BTC for $\Omega/\kappa = 5$: Shown are the Fourier transform of the $z-$spin dynamics for $N = 50$ spins, showing the peak at the first harmonic. Next, shows is the maximum value of the Fourier spectrum for increasing N, showing a logarithmic scaling with N.

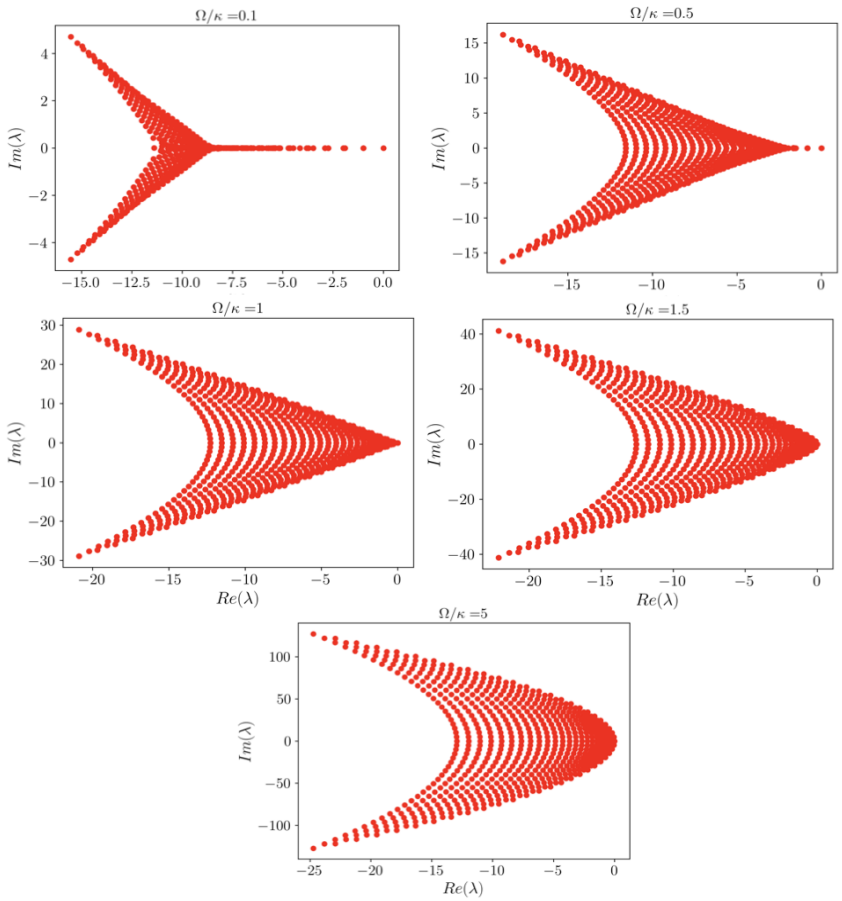

Figure 9: Liouvillian Eigenspectrum

crystal phase. The time crystal behaviour is clearly seen in Fig.7, with oscillations becoming sharper as N is increased, and finite size effect occuring for small $|\Omega/\kappa - 1|$.

To further quantify the thermodynamic argument, we study the Fourier spectrum of the magnetization dynamics, for $N = 50$ spins in Fig.8, which shows peaks at the first harmonic. A plot of the magnitude of these peaks for increasing N is in the second panel of Fig.8, which shows that the peaks increase logarithmically with N.

Interestingly, these dynamic behaviours and the BTC phase transition can also be analyzed from the point of view of the Liouvillian eigenspectrum. For the dissipative phase, there exists a unique steady state with zero imaginary eigenvalue corresponding to all spins down. Whereas, in the BTC phase, the spectrum consists of *oscillatory coherences*, taking the form of a degenerate steady space with $\pm\iota\lambda_0$ eigenvalues with $\lambda_0 \neq 0$. This imaginary eigenvalue causes the oscillations. Formally, we recall that the Liouvillian superoperator can be diagonalized,

$$\mathcal{L}\sigma^n = \lambda_n \sigma^n \tag{2.8}$$

and the steady state corresponds to σ^0 with $Re(\lambda_0) = 0$ (for if $Re(\lambda_0) \neq 0, e^{\lambda_0 t} \to 0$ as $\rho(t) := e^{\mathcal{L}t}\rho(0)$). Numerically, this is shown in Fig.9, where the transition is

clearly visible.

References

[BCA20] Yimu Bao, Soonwon Choi, and Ehud Altman. "Theory of the phase transition in random unitary circuits with measurements". In: *Physical Review B* 101.10 (2020), p. 104301.

[BP02] Heinz-Peter Breuer and Francesco Petruccione. *The theory of open quantum systems*. Oxford University Press, USA, 2002.

[CTDL19] Xiangyu Cao, Antoine Tilloy, and Andrea De Luca. "Entanglement in a fermion chain under continuous monitoring". In: *SciPost Physics* 7.2 (2019), p. 024.

[Cho+20] Soonwon Choi et al. "Quantum error correction in scrambling dynamics and measurement-induced phase transition". In: *Physical Review Letters* 125.3 (2020), p. 030505.

[DD16] Shrabanti Dhar and Subinay Dasgupta. "Measurement-induced phase transition in a quantum spin system". In: *Physical Review A* 93.5 (2016), p. 050103.

[GH20] Michael J Gullans and David A Huse. "Dynamical purification phase transition induced by quantum measurements". In: *Physical Review X* 10.4 (2020), p. 041020.

[HBD22] Tomohiro Hashizume, Gregory Bentsen, and Andrew J Daley. "Measurement-induced phase transitions in sparse nonlocal scramblers". In: *Physical Review Research* 4.1 (2022), p. 013174.

[Iem+18] F Iemini et al. "Boundary time crystals". In: *Physical review letters* 121.3 (2018), p. 035301.

[IK23] Matteo Ippoliti and Vedika Khemani. "Learnability transitions in monitored quantum dynamics via eavesdropper's classical shadows". In: *arXiv preprint arXiv:2307.15011* (2023).

[Jia+20] Chao-Ming Jian et al. "Measurement-induced criticality in random quantum circuits". In: *Physical Review B* 101.10 (2020), p. 104302.

[KMS19] Vedika Khemani, Roderich Moessner, and SL Sondhi. "A brief history of time crystals". In: *arXiv preprint arXiv:1910.10745* (2019).

[Kol23] Michael Kolodrubetz. "Optimality of Lindblad unfolding in measurement phase transitions". In: *Physical Review B* 107.14 (2023), p. L140301.

[LCF18] Yaodong Li, Xiao Chen, and Matthew PA Fisher. "Quantum Zeno effect and the many-body entanglement transition". In: *Physical Review B* 98.20 (2018), p. 205136.

[LCF19] Yaodong Li, Xiao Chen, and Matthew PA Fisher. "Measurement-driven entanglement transition in hybrid quantum circuits". In: *Physical Review B* 100.13 (2019), p. 134306.

[Li+23] Yaodong Li et al. "Cross entropy benchmark for measurement-induced phase transitions". In: *Physical Review Letters* 130.22 (2023), p. 220404.

[Mon+23] Victor Montenegro et al. “Quantum metrology with boundary time crystals”. In: *Communications Physics* 6.1 (2023), p. 304.

[Pic+21] Giulia Piccitto et al. “Symmetries and conserved quantities of boundary time crystals in generalized spin models”. In: *Physical Review B* 104.1 (2021), p. 014307.

[SRN19] Brian Skinner, Jonathan Ruhman, and Adam Nahum. “Measurement-induced phase transitions in the dynamics of entanglement”. In: *Physical Review X* 9.3 (2019), p. 031009.

[ST22] Jacopo Surace and Luca Tagliacozzo. “Fermionic Gaussian states: an introduction to numerical approaches”. In: *SciPost Phys. Lect. Notes* (2022), p. 54. DOI: 10.21468/SciPostPhysLectNotes.54. URL: https://scipost.org/10.21468/SciPostPhysLectNotes.54.

[WM09] Howard M Wiseman and Gerard J Milburn. *Quantum measurement and control*. Cambridge university press, 2009.

[Zho23] Yi-Neng Zhou. “Generalized Lindblad master equation for measurement-induced phase transition”. In: *SciPost Physics Core* 6.1 (2023), p. 023.

§A. Large scale stabilizer simulations

Here, we discuss the methodology of Clifford simulations under the hood of the stabilizer 'trick'. It turns out, instead of representing a state of n qubits with $\mathcal{O}(2^n)$ resources as one would naïvely think, one can represent a fairly large class of states with $\text{POLY}(n)$ resources and still get a good idea of the dynamics in a quantum system. This is using the Clifford algebra – circuits generated by CNOTs, Hadamards and Phase gates (CHP) can be simulated with polynomial resources.

Formally, for every Clifford state $|\psi\rangle$, there exists a sub-group $\mathcal{S} \subset \mathcal{P}_n$ of the Pauli group, such that

$$g|\psi\rangle = +|\psi\rangle \ \forall g \in \mathcal{S} \tag{A.1}$$

that is, the group $\mathcal{S}$ *stabilizes* $|\psi\rangle$. This group is unique given such a state, and this idea is used the other way around in quantum error correction, where a stabilizer group fixes a set of states called codewords used for encoding quantum information.

Since there are 2^n degrees of freedom in a general ket, to specify a single one we need 2^n conditions, and thus we would need

$$|\mathcal{S}| = 2^n \tag{A.2}$$

Intuitively, note that partitioning the Hilbert space into ± 1 partitions labelled by the eigenvalue of some $g \in \mathcal{P}_n$ divides it into two parts, and thus we require n total stabilizer generators to get a unique state after partitioning multiple times. Thus, the stabilizer group of 2^n is generated by n stabilizer generators (which we just refer to as generators) $g_1, \ldots, g_n$. It is this nice group theoretic structure which enables polynomial resource simulation of Clifford circuits. Moreover, a general $g \in \mathcal{S}$ can be written as,

$$g = g_1^{p_1} g_2^{p_2} \cdots g_n^{p_n} \tag{A.3}$$

with $p_i \in \{0, 1\}$, establishing a clean bijection between $\mathcal{S}$ and $\{0, 1\}^n$, and reaffirming that $|\mathcal{S}| = 2^n$. Note that for any stabilizer group, we must have that (i) it is Abelian, and (ii) $-I \notin \mathcal{S}$. The reader is left to answer why.

Entanglement in the stabilizer formalism. Recall that the von-Neumann entanglement entropy is defined as,

$$S_A := -Tr(\rho_A \log_2 \rho_A) \tag{A.4}$$

whereas the Rényi entropies are given as,

$$S_A^n := \frac{1}{1-n} \log_2 Tr(\rho_A)^n \tag{A.5}$$

for $n \in (0, 1) \cup (1, \infty)$, where $A \subset [n]$ is the one of the bipartitions of the n qubit system. For stabilizer states, all the Rényi entropies are equal, and are given as

$$S_A = |A| - \log_2 |\mathcal{S}_A| \tag{A.6}$$

where $\mathcal{S}_A$ is the subgroup of S that act trivially on $\bar{A}$ (i.e., $g_A \otimes 1_{\bar{A}} \in \mathcal{S}_A$). Equivalently,

$$S_A = |A| - |\mathcal{G}(\mathcal{S}_A)| \tag{A.7}$$

where $\mathcal{G}(\mathcal{S}_A)$ is an arbitrary generating set of $\mathcal{S}_A$.

Another formula for the entropies can be derived by defining a linear operator proj_A such that $\text{proj}_A(\mathcal{S})$ contains all the elements from $\mathcal{S}$ with their action on $\bar{A}$ set to triviality. Thus, $|\mathcal{G}(\mathcal{S}_A)| = \dim(\text{Ker}(\text{proj}_{\bar{A}}))$. Further by the rank nullity theorem, we then have [LCF19]

$$\begin{aligned} S_A &= |A| - \dim(\text{Ker}(\text{proj}_{\bar{A}})) && \text{(A.8)} \\ &= |A| - (n - \dim(\text{Im}(\text{proj}_{\bar{A}}))) && \text{(A.9)} \\ &= \dim(\text{Im}(\text{proj}_{\bar{A}})) - |\bar{A}| && \text{(A.10)} \end{aligned}$$

We can interchange $A \longleftrightarrow \bar{A}$ and get that

$$\boxed{S_A = |A| - \log_2 |\mathcal{S}_A| = \text{rank}(\text{proj}_A(\mathcal{S})) - |A|} \tag{A.11}$$

§B. Simulating monitored free-fermions

We follow the approach in [CTDL19]. A free fermion chain under monitoring of local occupation numbers (note that $n_i = 1 \cdot P_i^{(1)} + 0 \cdot P_i^{(0)}$ and $n_i^2 = n_i$) preserves Gaussianity of an initially Gaussian wavefunction, allowing for efficient numerical simulations. A Gaussian state is fully characterized by its two-point correlation function,

$$D_{ij}(t) = \langle c_i^\dagger c_j \rangle_t \tag{B.1}$$

The stochastic evolution equation coupled with Wick's theorem provides the evolution for the correlator as

$$dD = -\iota[h, D]dt - \gamma(D - D^{diag}) + \sqrt{\gamma}[DdW + dWD - 2DdWD] \tag{B.2}$$

where h is the tri-diagonal hopping matrix, D^{diag} is the diagonal matrix of D, and $W_{kl} = \delta_{kl} W^l$. Particularly, given N particles on a L-length chain (thus a filling factor of N/L), we represent the state by a $L \times N$ matrix as follows [CTDL19]

$$|\psi\rangle \equiv |U\rangle := \Pi_{k=1}^{N} \left[\sum_{j=1}^{L} U_{jk} c_j^\dagger \right] |\Omega\rangle \tag{B.3}$$

with $|\Omega\rangle$ being the vacuum state. The paranthesis above creates a single fermion across the chain with amplitudes given by the elements of U, and there are N such creations in total, as represented by the Π. This requires that U is an isometry: $U^\dagger U = 1$. Now, we will trotterize the SSE. Recall,

$$d|\psi_t\rangle = -\iota H dt |\psi_t\rangle + \sum_{i=1}^{L} \left(\sqrt{\gamma}(n_i - \langle n_i \rangle) dW_t^i - \frac{\gamma}{2}(n_i - \langle n_i \rangle_t)^2 dt \right) |\psi_t\rangle \tag{B.4}$$

Absorbing the $\sqrt{\gamma}$ inside the Wiener variables, a trotterization gives us,

$$|\psi_{t+\delta t}\rangle \sim e^{\sum_j [dW_t^j + (2\langle n_j \rangle_t - 1)\gamma dt)] n_j} \cdot e^{-\iota H dt} |\psi_t\rangle \tag{B.5}$$

Thus, we update the U as follows:

$$V_{t+dt} := M \cdot e^{-\iota h dt} U_t \tag{B.6}$$

where

$$M_{jk} = \delta_{jk} e^{\delta W_t^j + (2\langle n_j \rangle_t - 1)\gamma dt} \tag{B.7}$$

Perform a QR decomposition as $V_{t+dt} = QR$ and set $U_{t+dt} := Q$ which restores the isometry. The authors of [CTDL19] point out that this method does *not* necessitate a very small dt in the numerics.

Moreover, do note that the computation of the entanglement entropy for Gaussian states can be done by writing out the *reduced* correlation matrix of the bipartition, computing its eigenspectrum $\{\xi_i\}$, resulting in,

$$S = -\sum \xi_i \log \xi_i + (1 - \xi_i) \log (1 - \xi_i) \tag{B.8}$$

A detailed account of numerical approaches for studying fermionic systems can be found in the excellent reference [ST22].